International Journal of Heat and Mass Transfer 52 (2009) 1214–1222

Contents lists available at ScienceDirect

International Journal of Heat and Mass Transfer

journal homepage: www.elsevier.com/locate/ijhmt

Numerical investigation on combined multiple shell-pass shell-and-tube heat exchanger with continuous helical baffles

Qiuwang Wang *, Qiuyang Chen, Guidong Chen, Min Zeng

State Key Laboratory of Multiphase Flow in Power Engineering, Xi'an Jiaotong University, Xi'an 710049, China

ARTICLE INFO

Article history:
Received 16 May 2008
Received in revised form 8 September 2008
Available online 24 October 2008

Keywords:
Continuous helical baffle
Combined multiple shell-pass shell-and-tube heat exchanger (CMSP-STHX)
Segmental baffled shell-and-tube heat exchanger (SG-STHX)

ABSTRACT

A combined multiple shell-pass shell-and-tube heat exchanger (CMSP-STHX) with continuous helical baffles in outer shell pass has been invented to improve the heat transfer performance and simplify the manufacture process. The CMSP-STHX is compared with the conventional shell-and-tube heat exchanger with segmental baffles (SG-STHX) by means of computational fluid dynamics (CFD) method. The numerical results show that, under the same mass flow rate M and overall heat transfer rate Q_m, the average overall pressure drop Δp_m of the CMSP-STHX is lower than that of conventional SG-STHX by 13% on average. Under the same overall pressure drop Δp_m in the shell side, the overall heat transfer rate Q_m of the CMSP-STHX is nearly 5.6% higher than that of SG-STHX and the mass flow rate in the CMSP-STHX is about 6.6% higher than that in the SG-STHX. The CMSP-STHX might be used to replace the SG-STHX in industrial applications to save energy, reduce cost and prolong the service life.

1. Introduction

A variety of heat exchangers are used in industries, such as shell-and-tube heat exchangers, plate-fin heat exchangers, fin-and-tube heat exchangers, etc. The shell-and-tube heat exchanger (STHX) has relatively simple manufacture and multi-purpose application possibilities for gaseous and liquid media in a large temperature and pressure range, so they are still widely used in chemical industry, power production, food industry, environment engineering, waste heat recovery, air-conditioning, refrigeration and so on.

However, the traditional shell-and-tube heat exchanger with segmental baffles have many disadvantages [1,2]: (1) high pressure drop on the shell side due to the sudden contraction and expansion of the flow in the shell side, and the fluid impinging on the shell walls caused by segmental baffles; (2) low heat transfer efficiency due to the flow stagnation in the so-called "dead zones", which are located at the corners between baffles and shell wall; (3) low shell-side mass velocity across the tubes due to the leakage between baffles and shell wall caused by inaccuracy in manufacturing tolerance and installation; (4) short operation time due to the vibration caused by the shell-side flow normal to tube banks. When the traditional segmental baffles are used in STHX, higher pumping power is often needed to offset the higher pressure drop under the same heat load. Therefore, it is essential to develop a new type of STHX using different types of baffles to have higher heat transfer efficiency and lower pressure drop.

Over these decades, different kinds of STHX have been developed and better understanding has been achieved. Many various baffle types have been designed to enhance the shell-side heat transfer performance, for example, the rod baffles, the helical baffles, the deflecting baffles, disk-and-doughnut baffles [3], the twisted-tube heat exchanger, the corrugated-tube heat exchanger [4] and so on.

Helical baffles offer a possible alternative to segmental baffles by circumventing the aforementioned problems of conventional segmental baffles [5–7]. Different types of helical baffles can be found in reference [8] and shown in Fig. 1. Properly designed helical baffles are able to reduce fouling in the shell side [9] and prevent the flow-induced vibration [4,10]. Many researches have reported that the STHXs with helical baffles can reduce the vibrations [1–3]. In the shell side of traditional STHX with segmental baffles, the flow crosses the tube bundle vertically and may induce undesirable vibrations. In the STHX with helical baffles, the helical flow crosses the tube bundle in a certain angle relative to the axis and can greatly reduce vibrations. Andrews [11] have performed detailed three-dimensional computational fluid dynamics (CFD) simulations to explore the performance of a helical baffled heat exchanger. Zhang et al. [12] have enhanced the heat transfer performance of helical baffled heat exchanger combined with petal-shaped finned tubes and studied its heat transfer and pressure loss experimentally. Stehlik et al. [13] have compared heat transfer characteristics between helical baffled heat exchanger and segmental baffled heat exchanger. Results from single-phase heat

* Corresponding author.
E-mail address: wangqw@mail.xjtu.edu.cn (Q.W. Wang).

0017-9310/$ - see front matter © 2008 Elsevier Ltd. All rights reserved.
doi:10.1016/j.ijheatmasstransfer.2008.09.009

Nomenclature

A	heat transfer area, m^2, $N_t \pi D_t L$
c_i	coefficients in the k-ε turbulence model
c_p	specific heat, J/(kg K)
D_e	hydraulic diameter, mm
D_{in}, D_{out}	diameters of inlet tube and outlet tube, mm
D_{is},D_{os}	diameters of inner and outer shell, mm
Δp_m	pressure drop, Pa
D_t	diameter of heat exchange tubes, mm
h	average heat transfer coefficient, W/(m^2 K), $q_m/\Delta T$
H_b	baffle pitch, mm
I	turbulence intensity
k	turbulent fluctuation kinetic energy, m^2/s^2
L	tube length, mm
M	mass flow rate, kg/s
N_t	number of tubes
p_{out}	outlet pressure, Pa
Q	heat transfer rate, W, $c_p M (T_{out} - T_{in})$
x, y, z	coordinate, mm
Re	Reynolds number, $\rho u_m D_e/\mu$
S	source term
ΔT	log mean temperature difference, K, $(T_{out} - T_{in})/\ln[(T_w - T_{in})/(T_w - T_{out})]$
T_f	average temperature of fluid, K, $(T_{in} + T_{out})/2$
T_{in}	inlet temperature, K
T_{out}	outlet temperature, K
T_w	tube wall temperature, K
u, v, w	velocities in different directions, m/s
u_m	average velocity of fluid in shell side
x^+, y^+	dimensionless distance from the wall

Greek symbols

β	helix angle, °, $\text{atan}(2H_b/\pi D_{os})$
ρ	density, kg/m^3
λ	thermal conductivity, W/(m K)
Γ	generalized diffusion coefficient
ε	turbulent kinetic energy dissipation rate, m^2/s^3
μ	dynamic viscosity of fluid, kg/(m·s)
μ_t	turbulent dynamic viscosity, kg/(m s)
$_t$	turbulent kinematic viscosity, m^2/s
σ	thickness of sleeve tube, mm
σ_k	Prandtl number for k
σ_ε	Prandtl number for ε
φ	variables in generalized equations

transfer and pressure drop tests performed on heat exchanger with helical baffles show considerable advantage in shell side.

In the above motioned researches, in order to overcome the difficulty in the manufacturing, the discontinuous helical baffles are formed by lapped over fan or oval shaped plates, which are easy to be manufactured. The baffles are normally arranged by a central pole, of which the volume of the central pole is small, however, the leakage by discontinuous helical baffle is relatively large due to the triangle zones, which will reduce the heat transfer performance. To overcome the above defects, Wang et al. [8,14–16] have introduced a manufacture method for continuous helical baffles and found that the heat exchangers with continuous helical baffles are superior to the heat exchangers with segmental baffles or overlap helical baffles. But the manufacture of continuous helical baffles is relatively complicated than that of discontinuous helical baffles.

On the other hand, it is also found that the helical baffled heat exchanger has higher heat transfer performance only under same pressure drop. Under the identical tube arrangement, the identical shell size and identical mass flow rate, the helical baffled heat exchanger has relatively lower pressure drop in the shell side, but it has even lower heat transfer rate simultaneously, which is not always acceptable.

In order to simply the manufacture and make full use of the advantages of helical baffles, Wang et al. [17–20] have invented the combined multiple shell-pass heat exchangers with continuous helical baffles (CMSP-STHX) (see Fig. 2). This CMSP-STHX separates the shell side into several individual shell passes. As to each individual shell pass, the cross-sectional flow area is reduced, the velocity of fluid is increased and the heat transfer performance can have a great improvement. The two shell-pass CMSP-STHX is shown in Fig. 2. The inner shell pass is conventional segmental baffled, and the outer shell pass is helical baffled, which can greatly avoid the difficulty of the helical baffles manufacturing in the region of small shell diameter. In addition, the continuous helical baffles in the outer shell pass can reduce the pressure drop and mitigate fouling in the shell side and increase compactness of the STHX and prolong the service life of STHX.

In this study, in order to validate the advantages of CMSP-STHX, the comprehensive performance of the CMSP-STHX has been compared with that of a conventional STHX with segmental baffles (SG-STHX) by computational fluid dynamics (CFD) method. The commercial software FLUENT was used and all computations were performed on a personal computer with 8GB RAM and Intel® Core™ 2.40 GHz CPU.

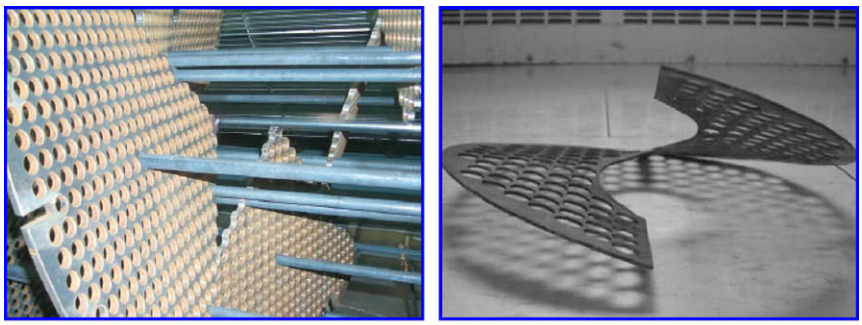

(a) discontinuous (b) continuous

Fig. 1. Different types of helical baffles.

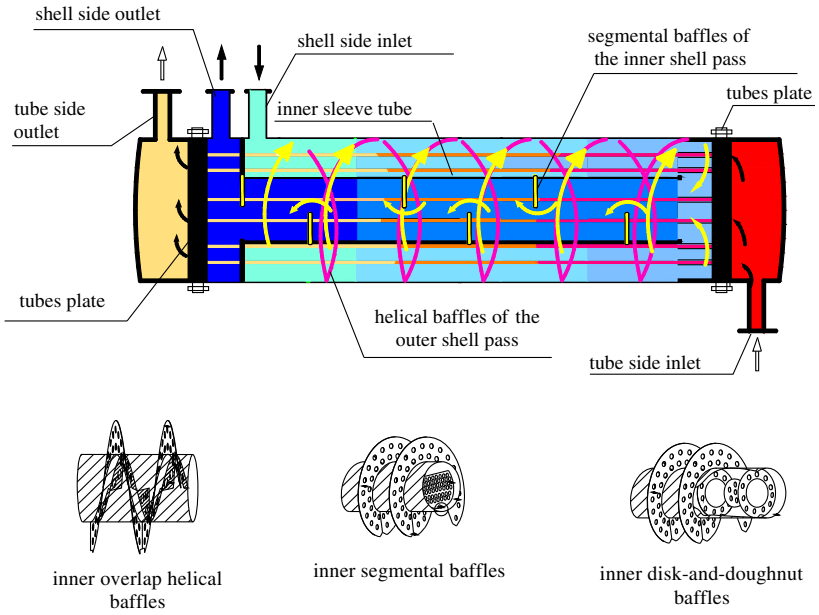

Fig. 2. Schematic of CMSP-STHX [19].

2. Models of shell-and-tube heat exchangers

2.1. Physical models

The physical model of CMSP-STHX to be studied is presented in Fig. 3(a), and the STHX with segmental baffles is presented in Fig. 3(b). The CMSP-STHX has two shell passes, the inner shell pass and the outer shell pass, which are separated by a sleeve tube. The inner shell pass is constructed by segmental baffles and the outer shell pass is constructed by complete continuous helical baffles. They join together at one end of the shell side. Detailed geometrical parameters of the computation models can be observed in Fig. 3.

The material of the sleeve tube is steel with thickness $\sigma = 2$mm, which has a density $\rho = 8030\ \mathrm{kg/m^3}$, thermal conductivity $\lambda = 16.27\ \mathrm{W/(m\ K)}$, and specific heat $c_p = 502.48\ \mathrm{J/(kg\ K)}$. The material of heat exchange tubes and baffles is aluminum, which has a density $\rho = 2719\ \mathrm{kg/m^3}$, thermal conductivity $\lambda = 202.4\ \mathrm{W/(m\ K)}$, and specific heat $c_p = 871\ \mathrm{J/(kg\ K)}$. The working fluid is water, whose thermal properties depend on the temperature.

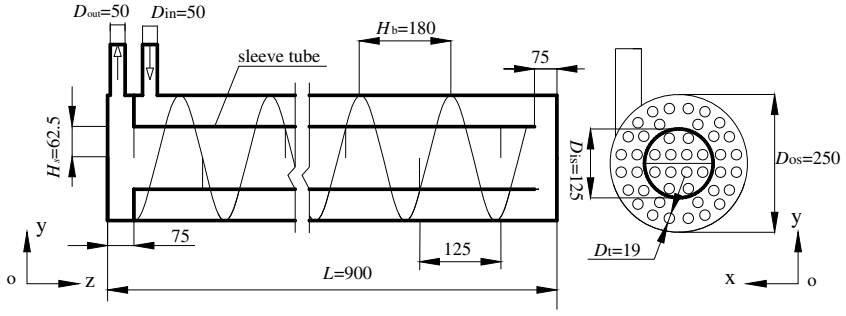

(a) CMSP-STHX

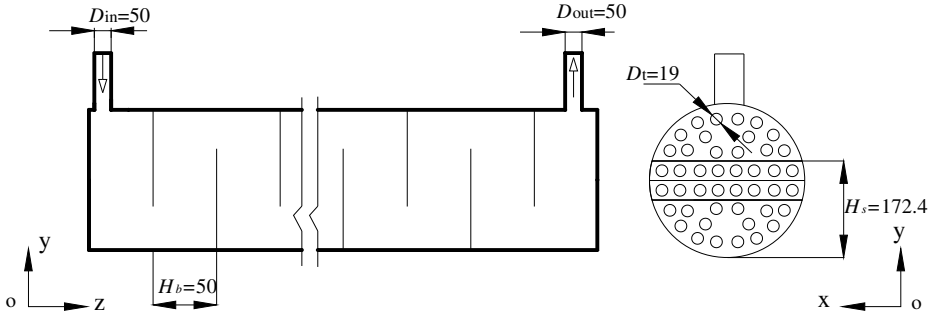

(b) SG-STHX

Fig. 3. Geometrical parameters of STHX models (unit: mm).

2.2. Governing equations

In order to simulate the flow and heat transfer in the shell side of STHXs, three-dimensional realizable k-ε turbulence models are applied.

The governing equations for different variables can be expressed as follows [21]:

Continuity equation

$$\frac{\partial u_i}{\partial x_i} = 0 \tag{1}$$

Momentum equation

$$\frac{\partial u_i u_j}{\partial x_i} = -\frac{\partial p}{\rho \partial x_i} + \frac{\partial}{\partial x_j}\left((v + v_t)\left(\frac{\partial u_j}{\partial x_i} + \frac{\partial u_i}{\partial x_j}\right)\right) \tag{2}$$

Energy equation

$$\frac{\partial u_i T}{\partial x_i} = \rho \frac{\partial}{\partial x_i}\left(\left(\frac{v}{Pr} + \frac{v_t}{Pr_t}\right)\frac{\partial T}{\partial x_i}\right) \tag{3}$$

Turbulent kinetic energy k equation

$$\frac{\partial u_i k}{\partial x_i} = \frac{\partial}{\partial x_i}\left(\left(v + \frac{v_t}{\sigma_k}\right)\frac{\partial k}{\partial x_i}\right) + \Gamma - \varepsilon \tag{4}$$

Rate of energy dissipation ε equation

$$\frac{\partial(\rho u_j)}{\partial x_j} = \frac{\partial}{\partial x_i}\left(\left(v + \frac{v_t}{\sigma_\varepsilon}\right)\frac{\partial \varepsilon}{\partial x_i}\right) + c_1 \Gamma \varepsilon - c_2 \frac{\varepsilon^2}{k + \sqrt{v\varepsilon}} \tag{5}$$

where Γ denotes the production rate of k and is given by

$$\Gamma = -\overline{u_i u_j}\frac{\partial u_i}{\partial x_i} = v_t\left(\frac{\partial u_i}{\partial x_j} + \frac{\partial u_j}{\partial x_i}\right)\frac{\partial u_i}{\partial x_i} \tag{6}$$

$$v_t = c_\mu \frac{k^2}{\varepsilon} \tag{7}$$

The coefficients in k-ε turbulence model are given as follows:

$$c_1 = \max[0.43, \mu/(\mu_t + 5)], c_2 = 1.0, \sigma_k = 1.0, \sigma_\varepsilon = 1.2$$

To achieve the realizability effect, the c_μ is no longer constant but a function of the turbulence fields, mean strain and rotation rates.

The standard wall function is adopted near the wall and the range of the dimensionless length x^+ or y^+ is $10 < x^+(y^+) < 100$.

2.3. Boundary conditions

The boundary conditions are described as follows:

(1) The shell inlet:
- $u = w = 0$, v = constant (uniform inlet velocity),
- T_{in} = 298K (25 °C) (uniform inlet temperature),

(2) The inlet turbulent kinetic energy k is calculated using:
- $k = \frac{3}{2} I^2 v^2$
- where I is the inlet turbulence intensity, I = 1%.

(3) The inlet dissipation ε is calculated using:
- $\varepsilon = \frac{c_\eta \rho k^2}{\mu_t}$
- where c_η is the turbulence coefficients, μ_t is the turbulent dynamic viscosity.

(4) The shell outlet:
- $\frac{\partial u}{\partial n} = \frac{\partial v}{\partial n} = \frac{\partial w}{\partial n} = 0, \frac{\partial T}{\partial n} = 0, \frac{\partial k}{\partial n} = 0, \frac{\partial \varepsilon}{\partial n} = 0$
- where n is the normal vector of outlet plane.

(5) The heat exchange tube wall surfaces:
- $u = v = w = 0$
- T_w = 373K (100 °C) (hot tube walls)

Note that for gases and liquids (Pr > 0.5), very little difference exists between the Nusselt number under uniform wall temperature boundary condition (B.C.) and that under uniform wall heat flux B.C. in turbulent flow [22]. Therefore, the effect of thermal boundary condition of tube surface on CFD results can be ignored. In the present work, since our main focus is the comparison of shell-side comprehensive performance between the combined multiple shell-pass STHX (CMSP-STHX) and the traditional segmental baffled STHX (SG-STHX), it is expected that the boundary condition will not affect the conclusion of the present study. Therefore, we impose the uniform wall temperature B.C. on the hot tube walls.

(6) The outer shell walls:
- u=v=w=0
- $\frac{\partial T}{\partial n} = 0$ (thermal insulation walls)

(7) The sleeve tube wall surface:
- $u = v = w = 0$

(8) The baffle walls:
- $u = v = w = 0$

Due to the conjugated heat transfer characteristics between the baffle walls surfaces, sleeve tube wall surfaces and the fluid, the thermal boundary conditions do not need to be specified on the interior of baffle wall surfaces and the sleeve tube walls surfaces.

2.4. Numerical methods

The computations are carried out using FLUENT, a commercial CFD code. The algorithm employed is SIMPLE. The second order upwind scheme is used for the numerical simulation. As for the convergence criterion, the sum of the normalized absolute residuals in each control volume for the flow variables are controlled to be less than 10^{-5} and 10^{-7} for energy variables. The CPU time of computation for typical case is about 30 h.

The Reynolds number is defined as

$$Re = \rho u_m D_e / \mu \tag{8}$$

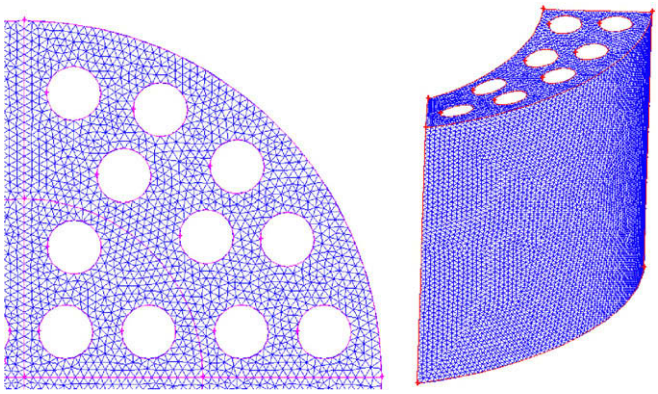

Fig. 4. Local schematic diagrams of grid.

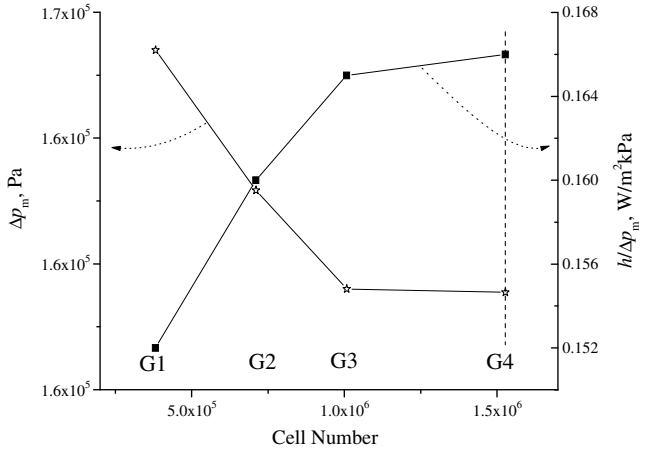

Fig. 5. Results of different grid systems (Re = 49,129).

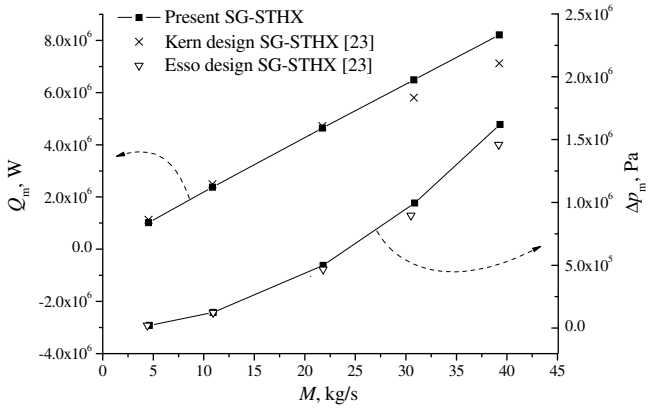

Fig. 6. Comparisons of the present results with the prediction of correlations.

where u_m is the average velocity of fluid in shell side, which can be obtained from computation results. The hydraulic diameter $D_e = D_t = 19$ mm. ρ is the density of water and μ is the dynamic viscosity of water. Both ρ and μ are both determined by the average temperature of the working fluid $T_f = (T_{in} + T_{out})/2$.

The overall heat transfer rate Q_m can be calculated from:

$$Q_m = c_p M(T_{out} - T_{in}) \quad (9)$$

where T_{in} and T_{out} are the bulk inlet and outlet water temperatures, respectively. M is the mass flow rate of working fluid.

The average heat transfer coefficient h is defined as

$$h = Q_m/(\Delta T A) \quad (10)$$

where ΔT is the log mean temperature difference and defined as $\Delta T = (T_{out} - T_{in})/\ln[(T_w - T_{in})/(T_w - T_{out})]$. There are totally N_t(=44) heat exchange tubes arranged in the shell side and the heat transfer area is $A = N_t \pi D_t L$.

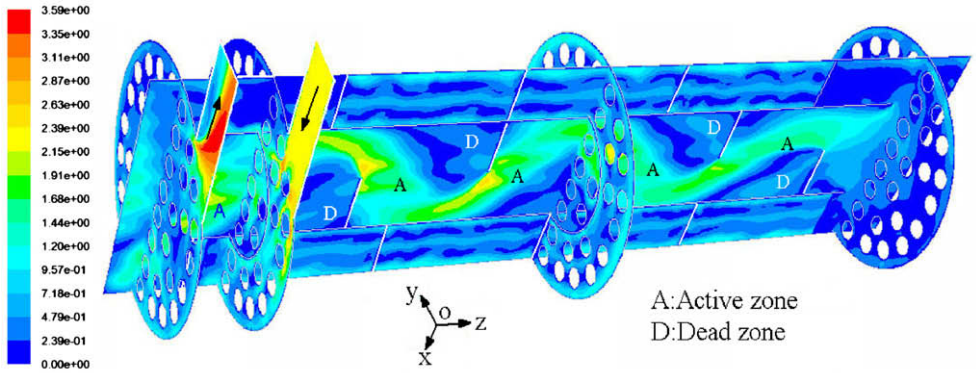

(a) CMSP-STHX

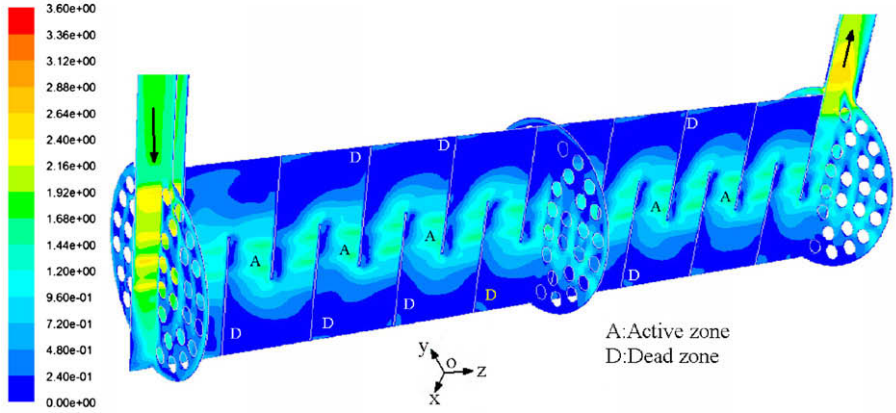

(b) SG-STHX

Fig. 7. Velocity distributions (β = 25°, M = 4.4 kg/s) (unit: m/s).

2.5. Grid systems

Due to the complicated structure of the CMSP-STHX, the computational domain is meshed with the unstructured Tet/Hybrid grids (see Fig. 4), which are generated by another commercial code GAMBIT. In order to ensure the accuracy of numerical results, a careful check for the grid independence of the numerical solutions was conducted. Four different grid systems are generated for the CMSP-STHX (Re = 49,129, M = 10.92 kg/s). The results are shown in Fig. 5. It is found that the relative deviation of the average heat transfer coefficient under unit overall pressure drop $h/\Delta p_m$ between G3 and G4 is less than 2%. The relative deviation of the overall pressure drop Δp_m between G3 and G4 is less than 3%. The final grid system for the studied cases is G4 with about 1.5×10^6 grid cells.

2.6. Validation of numerical model

In order to validate the numerical model, the Kern method [23] is used to calculate the overall heat transfer rate Q_m and the Esso method [23] is used to calculate the overall pressure drop Δp_m in the shell side of STHX with segmental baffles. Comparisons of the present results with the prediction of correlations are shown in Fig. 6. It is found that the average deviation of the overall heat transfer rate Q_m between present results and Kern design results is about 8.4%. On the other hand, the average deviation of the overall pressure drop Δp_m between present results and Esso design results is about 3.6%. Considering the error of heat transfer rate associated with the Kern design results and the error of pressure drop associated with the Esso design results (both less than 10%), it can be concluded that the present model can give a satisfactory prediction in both heat transfer and pressure drop characteristics.

3. Results and discussion

3.1. Velocity distributions

The velocity distributions of two STHXs are shown in Fig. 7 with same mass flow rate. It can be found that there is nearly no back flow regions existed in the outer shell pass of CMSP-STHX (β = 25°, M = 4.4 kg/s). On the one hand, helical flow rushes the heat exchange tubes with an inclination angle and then can reduce the vibration of tubes. On the other hand, it avoids abrupt turns of flow and reduces pressure drop in the shell side. In the inner shell pass of CMSP-STHX and SG-STHX, the fluid flows cross the heat exchange tubes and rushes toward the shell and baffles in a tortuous, zigzag manner, as expected.

3.2. Pressure distributions

The pressure distributions of two STHXs are shown in Fig. 8. For the CMSP-STHX, the partial pressure drop of inner shell pass (about 13,840 Pa) is higher than that of the outer shell pass (about 8600 Pa). The overall pressure drop Δp_m of the CMSP-STHX (about 22,440 Pa) is slightly lower than that of SG-STHX (about 24,440 Pa).

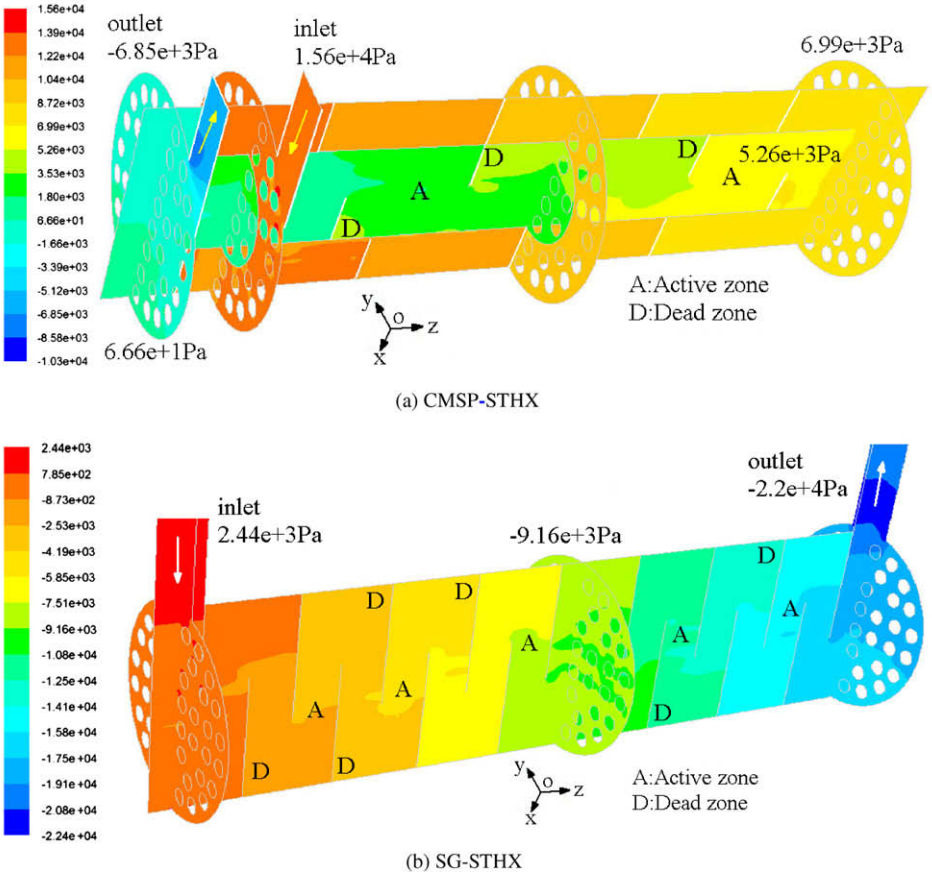

Fig. 8. Pressure distributions (β = 25°, M = 4.4 kg/s) (unit: Pa).

3.3. Temperature distributions

For the helical battled STHX, Peng et al. [8] found that the side-in-side-out inlet/outlet design is better than middle-in-middle-out inlet/outlet design. So the side-in-side-out inlet/outlet design is adopted in the present CMSP-STHX. The temperature distributions of two STHXs are shown in Fig. 9. From Fig. 9, it can be observed that in the outer shell pass of the CMSP-STHX, the temperature increases evenly and smoothly. The temperature difference in each helical cycle is small, and the temperature of heat exchange tubes is relatively uniform in each helical cycle. The relatively uniform temperature can prolong the service life of those tubes arranged in the outer shell pass. Because the number of heat exchange tubes located in the outer shell pass is larger than that in the inner shell pass, the working fluid has a 41K (339 − 298 = 41K) temperature increase in the outer shell pass, which is higher than that in the inner shell pass (the temperature increase in the inner shell pass is 15K (354 − 339 = 15K)). As expected, the inner shell pass has a relatively poor heat transfer performance due to the use of segmental baffles, but it can greatly reduce the manufacture difficulties. In the inner shell pass of CMSP-STHX and the SG-STHX, there are "dead zones" (marked by "D") and "active zones" (marked by "A"). The "Dead zones" have lower local heat transfer coefficients, because they can not exchange heat with the main flow freely. The "Active zones" can exchange heat with the main flow quickly. The local temperatures of "dead zones" are higher than those of "active zones", which means the temperature difference of heat exchange tubes is larger in each helix cycle. This may directly reduce heat transfer coefficient and may also reduce the service life.

3.4. Comparison of overall performance

In order to evaluate the overall performance of the studied two STHXs, we compared them under the same mass flow rate and the same overall heat transfer rate. The geometrical parameters of CMSP-STHX are fixed, and the pitch of baffles H_b of SG-STHX is adjusted to make these two STHXs have the same overall heat transfer rate Q_m (see Q_m curves in Fig. 10).

The variation of Q_m and Δp_m vs. mass flow rate M in the shell side are shown in Fig. 10. It is found that the maximum deviation of the overall heat transfer rate Q_m between these two STHXs is less than 0.8% when H_b = 50 mm. Therefore, it can be assumed that

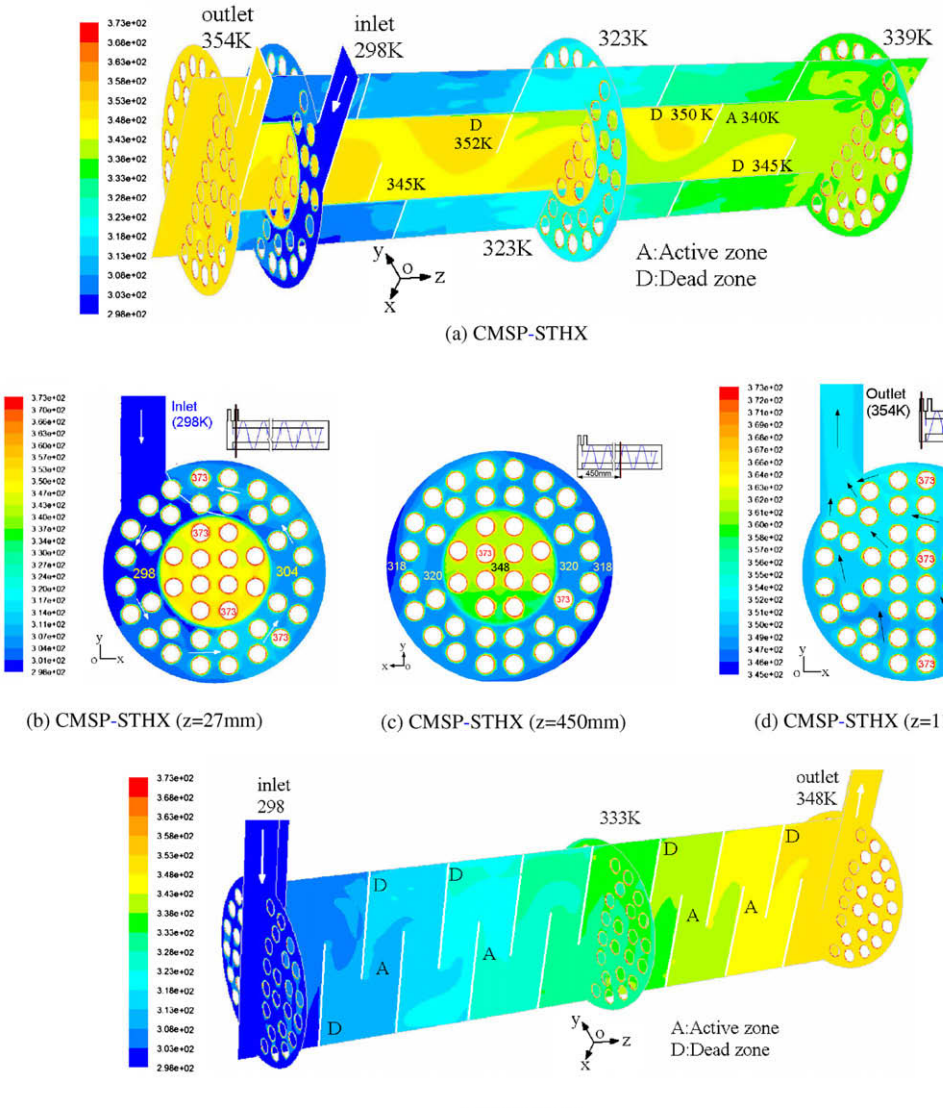

Fig. 9. Temperature distributions (β = 25°, M = 4.4 kg/s) (unit: K).

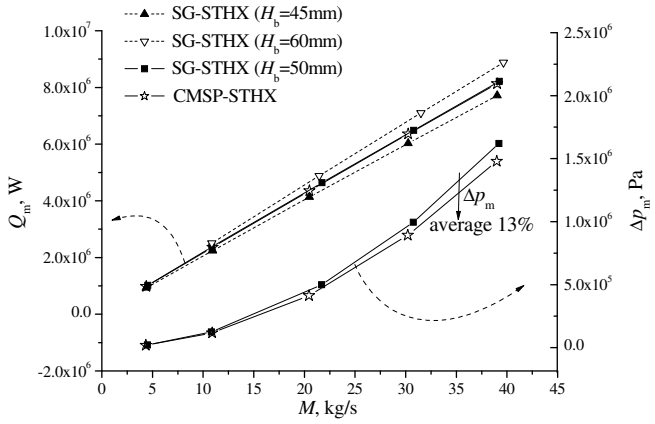

Fig. 10. Variation of Q_m and Δp_m vs. M.

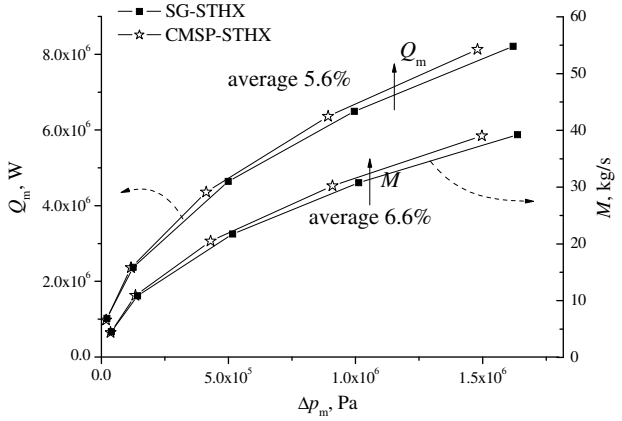

Fig. 11. Variation of Q_m vs. Δp_m ($\beta = 25°$).

the two SHTXs have the same overall heat transfer rate Q_m under the same mass flow rate M. On the other hand, the overall pressure drop Δp_m of the CMSP-STHX is about 13% lower than that of the SG-STHX under the same mass flow rate M and the same overall heat transfer rate Q_m.

The variation of the overall heat transfer rate of the heat exchangers Q_m with the overall pressure drop Δp_m is shown in Fig. 11. The results indicate that in the lower overall pressure drop region, the heat transfer rate Q_m has a fast increasing with the increase of overall pressure drop. While in the high pressure drop region, this increase trend becomes slow. Under the same overall pressure drop, the difference of the overall heat transfer rate of the STHXs is very small in the lower pressure drop region. However, in the higher pressure drop region, the overall heat transfer rate Q_m in the CMSP-STHX is obviously higher than that in the SG-STHX at the same overall pressure drop Δp_m. The average heat transfer rate Q_m in the CMSP-STHX is about 5.6% higher than that in the SG-STHX. Meanwhile, under the same overall pressure drop Δp_m, the mass flow rate in the CMSP-STHX is about 6.6% higher than that in the SG-STHX.

3.5. The choice of inner shell pass with segmental baffles

The reason why we do not use the helical baffles in the inner shell pass is that it is quite difficult to manufacture the helical baffle in the central part of the shell. In fact, several attempts [18,19,24] have tried to avoid the difficulties in manufacturing continuous helical baffles with a small scale inner helix edge and simplifies the manufacture of heat exchanger with continuous helical baffles. It also makes use of the space in the central pole, which is used to form the inner helix in the single shell-pass STHX with continuous helical baffles.

Therefore, considering the advantages and disadvantages of continuous helical baffles and the segmental baffles, it is valuable to separate the shell side into two different shell passes. Segmental baffle is still a better choice for the inner shell pass, because it can be manufactured and installed easily in a relatively small space.

4. Conclusions

In the present paper, a combined multiple shell-pass STHX with continuous helical baffles in the outer shell pass (CMSP-STHX) is investigated with CFD method and compared with a single shell pass STHX with segmental baffles (SG-STHX). The conclusions are summarized as follows:

(1) Under the same mass flow rate M and overall heat transfer rate Q_m, the average overall pressure drop Δp_m of the CMSP-STHX is lower than that of SG-STHX by 13%.
(2) Under the same overall pressure drop Δp_m in the shell side, the overall heat transfer rate Q_m of the CMSP-STHX is nearly 5.6% higher than that of conventional SG-STHX and the mass flow rate in the CMSP-STHX is about 6.6% higher than that in the SG-STHX.

Acknowledgments

This work is supported by National Science and Foundation of China (grant no. 50776068) and Program for New Century Excellent Talents in University of China (grant no. NCET-04-0938).

References

[1] H.D. Li, V. Kottke, Effect of the leakage on pressure drop and local heat transfer in shell-and tube heat exchangers for staggered tube arrangement, Int. J. Heat Mass Transfer 41 (2) (1998) 425–433.
[2] H.D. Li, V. Kottke, Visualization and determination of local heat transfer coefficients in shell-and-tube heat exchangers for staggered tube arrangement by mass transfer measurements, Exp. Therm. Fluid Sci. 17 (3) (1998) 210–216.
[3] H.D. Li, V. Kottke, Analysis of local shellside heat and mass transfer in the shell-and-tube heat exchanger with disc-and-doughnut baffles, Int. J. Heat Mass Transfer 42 (18) (1999) 3509–3521.
[4] P. Stehlik, V.V. Wadekar, Different strategies to improve industrial heat exchange, Heat Transfer Eng. 23 (6) (2002) 36–48.
[5] B.I. Master, K.S. Chunangad, A.J. Boxma, D. Kral, P. Stehlik, Most frequently used heat exchangers from pioneering research to worldwide applications, Heat Transfer Eng. 27 (6) (2006) 4–11.
[6] D. Kral, P. Stehlik, H.J. Van der Ploeg, B.I. Master, Helical baffles in shell-and-tube heat exchangers, Part I: Experimental verification, Heat Transfer Eng. 17 (1) (1996) 93–101.
[7] Q.W. Wang, Current status and development of shell-side heat transfer enhancement of shell-and-tube heat exchangers with helical baffles, J. Xi'an Jiaotong Univ. 38 (9) (2004) 881–886 (in Chinese).
[8] B. Peng, Q. W Wang, C. Zhang, G.N. Xie, L.Q. Luo, Q.Y. Chen, M. Zeng, An experimental study of shell-and-tube heat exchangers with continuous helical baffles, J. Heat Transfer (Trans. ASME) 129 (10) (2007) 1425–1431.
[9] I.M. Bashir, S.C. Krishnan, P. Venkateswaran, Fouling Mitigation using Helixchanger Heat Exchangers, ECI Conference on Heat Exchanger Fouling and Cleaning: Fundamentals and Applications, Santa Fe, New Mexico, USA, May 2003.
[10] D. Butterworth, Developments in shell-and-tube exchangers, Inst. Chem. Eng. Symp. Series 1 (129) (1992) 409–415.
[11] M.J. Andrews, B.I. Master, Three-dimensional modeling of a helixchanger heat exchanger using CFD, Heat Transfer Eng. 26 (6) (2005) 22–31.
[12] Z.G. Zhang, T. Xu, X.M. Fang, Experimental study on heat transfer enhancement of a helically baffled heat exchanger combined with three-dimensional finned tubes, Appl. Therm. Eng. 24 (14–15) (2004) 2293–2300.
[13] P. Stehlik, J. Nemcansky, D. Kral, L.W. Swanson, Comparison of correction factors for shell-and-tube heat exchangers with segmental or helical baffles, Heat Transfer Eng. 15 (1) (1994) 55–65.
[14] Q.W. Wang, G.N. Xie, M. Zeng, L.Q. Luo, Prediction of heat transfer rates for shell-and-tube heat exchangers by artificial neural networks approach, J. Therm. Sci. 15 (3) (2006) 257–262.

[15] Q.W. Wang, G.N. Xie, B.T. Peng, M. Zeng, Experimental study and genetic-algorithm-based correlation on shell-side heat transfer and flow performance of three different types of shell-and-tube heat exchangers, J. Heat Transfer (Trans. ASME) 129 (9) (2007) 1277–1285.
[16] G.N. Xie, Q.W. Wang, M. Zeng, L.Q. Luo, Heat transfer analysis for shell-and-tube heat exchangers with experimental data by artificial neural networks approach, Appl. Therm. Eng. 27 (5–6) (2007) 1096–1104.
[17] Q.W. Wang, Q.Y. Chen, M. Zeng, Y.N. Wu, L.Q. Luo, China Patent, ZL200610041949.1, 2006.
[18] Q.W. Wang, Q.Y. Chen, M. Zeng, Y.N. Wu, Q. Gao, China Patent, ZL200710017478.5, 2007.
[19] Q. W. Wang, Q.Y. Chen, D.J. Zhang, M. Zeng, Y.N. Wu, Q. Gao, US Patent, Pub. No. US2008/0190593A1, 2008.
[20] Q.W. Wang, Investigation on novel combined multiple shell-pass shell-and-tube heat exchangers with helical baffles, Workshop on advances in compact and micro heat exchangers for sustainable development, IIT Delhi, India, January 2008.
[21] T.H. Shih, W.W. Liou, A. Shabbir, J.A. Zhu, New k-ε eddy-viscosity model for high Reynolds number turbulent flows-model development and validation, Comput. Fluids 24 (3) (1995) 227–238.
[22] W.M. Rohsenow, J.P. Hartnett, Y. Cho, Handbook of Heat Transfer, McGraw-Hill Handbooks, 1998. 5.22.
[23] T. Kuppan, Heat Exchangers Design Handbook, Marcel Dekker Inc., New York, 2002.
[24] Q.W. Wang, D.J. Zhang, M. Zeng, Y.N. Wu, Q. Gao, China Patent, 200710017395.6, 2007.